JOURNAL OF MATERIALS SCIENCE **39** (2004) 6529–6538

Fracture behavior of nylon hybrid composites

S. PISHARATH
School of Materials Engineering, Nanyang Technological University, Nanyang Avenue, Singapore 639798, Republic of Singapore

SHING-CHUNG WONG*
Department of Mechanical Engineering, University of Akron, Akron, OH 44325-3903, USA
E-mail: swong@uakron.edu

XIAO HU
School of Materials Engineering, Nanyang Technological University, Nanyang Avenue, Singapore 639798, Republic of Singapore

Hybrid composite systems consisting of liquid crystalline polymer (LCP), short glass fibers and toughened nylon in varied ratios were studied. Dynamic mechanical results indicated that, elastomeric phase in toughened nylon 6,6 promoted a better compatibilization between nylon 6,6 and LCP in a hybrid system containing short glass fibers in comparison with one without glass fibers. Improved compatibility facilitated fibrillation of LCP phase in the skin region of the hybrid composite, thereby providing superior tensile strength. Without the presence of LCP, glass fiber reinforced toughened nylon 6,6 exhibited the least tensile strength. *J*-integral analysis and essential work of fracture (EWF) method were used to compare the fracture behavior of composites. Results showed that specific essential work of fracture were consistent with the critical *J*-integral. Matrices reinforced by LCP alone showed the best crack initiation and propagation toughnesses, followed by glass fiber reinforced and hybrid composites. The better compatibility between nylon 6,6 and LCP appeared to inhibit the interfacial debonding process, resulting in brittle fracture.

1. Introduction

To circumvent the reduction in mechanical strength and stiffness due to rubber toughening, our previous work [1, 2] investigated the effect of composite hybridization on the processability, morphology and crystalline state of liquid crystalline polymer (LCP)-containing glass fiber reinforced toughened nylon 6,6. It was observed that LCP addition improved the processability of reinforced toughened nylon due to the orientational effect of LCP domains in the direction of flow. Our studies also indicated that, elastomers in toughened nylon 6,6 exhibited a compatibilizing role in enhancing interfacial interaction between nylon 6,6 and LCP leading to an improved tensile strength and modulus in 20 wt% LCP hybrid composite. Our work [1, 2] showed that hybrid composites gave rise to distinct benefits in materials development.

Comparative studies of LCP and glass fiber reinforcements for thermoplastic matrices [3] showed that tensile properties of composites derived from LCPs were comparable to those pertaining to glass fiber reinforced thermoplastics. However little attention has been given to a systematic comparison of fracture behavior of LCP and glass fiber reinforced toughened plastics. The objective of this paper is to investigate the fracture behavior and tensile properties of three characteristic hybrid systems, which are shown in Table I.

Fracture mechanics techniques including J-integral and essential fracture work were employed in the study of the hybrid composites. Morphology and fractography were done using scanning electron microscopy (SEM).

2. Experimental

2.1. Materials

The polymers used in this research were rubber toughened nylon 6,6 (Zytel ST801 from DuPont) and liquid crystalline polymer (LCP), (Vectra A950 from Hoechst Celanese). Zytel ST801 comprises nylon 6,6 with 20 vol% EPDM rubber particles. Vectra A950 is made up of 27-mol% 2-hydroxy-6-naphthoic acid (HNA) and 73-mol% *p*-hydroxybenzoic acid (HBA). The short glass fibers used were *E*-glass fibers with a length of 12 mm and a diameter of 17 μm.

*Author to whom all correspondence should be addressed.

TABLE I Blend compositions

Hybrid system	Glass fiber (wt%)[a]	LCP (wt%)	Toughened nylon 6,6 (wt%)
Sample A	0	20	80
Sample B	20	0	80
Sample C	20	20	60

[a]Average fiber length = 12 mm; Fiber diameter = 17 μm.

2.2. Specimen preparation

Blend compositions by weight are shown in Table I. Materials were pre-compounded using a high shear rate, inter-meshing, co-rotating twin-screw extruder (Leistritz Micro 18; with a screw diameter of 18 mm and L/D ratio = 30). In the extruder, barrel temperatures were set at 260/280/285/285/292°C and a screw speed of 200 rpm was used. The dried extruded pellets were injection molded into 3.5 mm thick dog bone specimens using a Battenfeld BA 300 CD^{Plus} injection-molding machine for tensile tests and 6.35 mm thick Izod bars for fracture mechanics study. The temperatures in zone 1 and zone 2 were kept at 285 and 292°C respectively. The nozzle temperature was kept at 275°C and the mold temperature at 30°C. An injection pressure of 70 bar and holding time of 50 s were used. Screw speed was kept at 140 rpm.

Single-edge notch-bend (SENB) specimens having dimensions of 55 × 6.35 ×12.5 mm^3 were used for J-integral fracture measurements. The specimens were machine notched using a saw. Precracks were introduced by tapping a fresh razor blade into the root of the machined notch. The crack length to width (a/W) ratio was controlled in the range of 0.55 to 0.65. Test specimens for essential fracture work measurements were prepared similarly. Specimens of different ligament lengths were obtained by varying the crack length to specimen width (a/W) ratio from 0.15 to 0.8. This was accomplished by changing the length of the machined notch. Prior to testing, all specimens were dried at 80°C under vacuum for 24 h and kept in a dry box at room temperature.

2.3. Dynamic mechanical analysis

Dynamic mechanical analysis was performed using TA DMA 2980 equipped with TA thermal analysis software. The measurements were made on injection-molded specimens at a scan rate of 3°C min^{-1} and a frequency of 1 Hz in a temperature range of −120 to 120°C. A double cantilever clamp in a bending mode was used for the tests.

2.4. Tensile tests

Tensile tests were conducted on 3.5 mm-thick dumbbell specimens with an Instron 5565 using a 30 kN load cell. Test speed was kept at 5 mm min^{-1}. An extensometer was used to precisely monitor the elastic modulus. Values reported were averages of at least 5 measurements.

2.5. Fracture toughness characterization

For J-integral fracture measurements, SENB specimens were loaded in three-point bend geometry following the ASTM Standad E813 and using an Instron 5565 at a crosshead speed of 5 mm min^{-1}. Span to width ratio (S/W) was maintained at 4 for all tests. After careful unloading, the specimens were immersed in liquid nitrogen for 20 min followed by fast fracturing. The stable crack growth was monitored using an OLYMPUS UH2 microscope fitted with a micrometer eyepiece. The J value was calculated by

$$J = \frac{2U}{B(W-a)} \tag{1}$$

where, U is the area under load-deflection curve, B the specimen thickness, W the width of the specimen and a the crack length. J thus calculated was plotted against the microscopically measured crack extension Δa, to obtain the $J_R - \Delta a$ curve. The J-R curve was constructed using a linear regression line. Fracture initiation toughness J_c was obtained from the y-intercept by extrapolating the linear J-R curve to zero crack growth. Validity of J_{Ic} was checked using the following criterion.

$$B \geq 25\left(\frac{J_c}{\sigma_y}\right) \tag{2}$$

where B is the specimen thickness and σ_y the yield stress, which in our case is the ultimate tensile strength. Tearing modulus, T was calculated from the slope of the J-R curve using the following equation.

$$T = \frac{E}{\sigma_y^2}\frac{dJ_R}{da} \tag{3}$$

where E is the young's modulus of the material, and $\frac{dJ_R}{da}$ is the beginning slope of J-R curve.

To measure the specific essential fracture work, w_e, SENB specimens with different ligament lengths were loaded in three-point bend geometry until the ligaments tore apart. The tests were done at a test speed of 5 mm min^{-1} and an S/W ratio = 4. Specific total fracture work, w_f, for each specimen was calculated using the following equation [4]:

$$w_f = w_e + \beta w_p \tag{4}$$

where w_e is the specific essential fracture work, w_p the geometry-dependent nonessential plastic work, and β the geometry factor. The plane strain essential fracture work, w_{Ie}, was verified when following criterion was met:

$$B \geq 25\left(\frac{w_e}{\sigma_y}\right) \tag{5}$$

2.6. Microscopy

The morphology of composite specimens was studied using a Jeol 5410LV scanning electron microscope (SEM). Injection molded specimens were cryogenically fractured after immersing them in liquid nitrogen

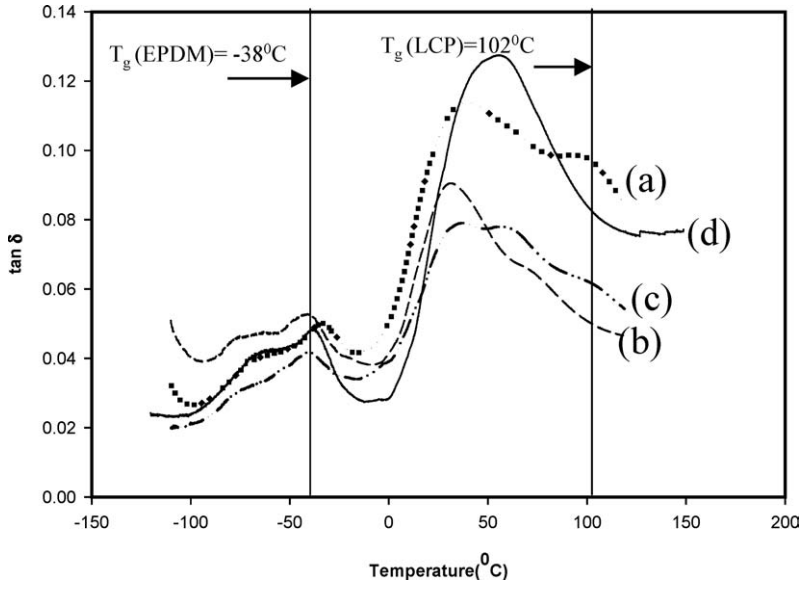

Figure 1 Dynamic mechanical spectra of (a) sample A, (b) sample B, (c) sample C, and (d) unreinforced rubber toughened nylon 6,6.

for 20 min and the surfaces were coated with a thin layer of gold using an SPI sputter coater.

For fiber orientation measurements, injection molded specimen was cut and embedded in the epoxy resin. The view surface was kept parallel to the mold filling direction (MFD). This epoxy block was polished to the mid section through the thickness. SEM micrographs were taken to show fiber orientation and distribution. The fiber orientation with respect to MFD was analyzed on the micrograph using an image analysis software (Image-Pro Plus, Media Cybernetics, L.P.). A Fortran computer program was used to measure the number of fibers in each of recurring angle intervals from the data obtained on the image analyzer. These numbers were expressed as a percentage frequency in each of the angle intervals by dividing the number with the total number of fibers used for measurements. The frequency was plotted against the angles to get the distribution of fiber orientation.

For fiber length measurements the glass fibers were isolated after burning the polymer matrix. The separated glass fibers were dispersed in a solution on a glass slide for observation under a light microscope (NIKON LABPHOT-2) equipped with an image analyzer (Image-Pro Plus, Media Cybernetics, L.P.). The number of fibers within regular length intervals was evaluated. The percentage frequencies were calculated and plotted against the fiber length to obtain the frequency distribution.

3. Results and discussion

3.1. Thermal analysis

Maleic anhydride grafted elastomers are widely used for toughening nylons [5]. Maleic anhydride groups are prone to undergo acidolysis reaction with the ester group present on the LCP, as well as aminolysis reaction with amine groups that are on nylon 6,6. The evolution of phase morphology is determined by the relative rate of these competitive reactions. Our previous work [2] indicated that such elastomers played a compatibilizing role between nylon 6,6 and LCP. DMA can provide useful information reflecting the interfacial interaction between the blend components.

Tan δ of rubber toughened nylon 6,6 and the hybrid composite systems studied are shown in Fig. 1. The tan δ peaks for the elastomeric phase in the toughened matrices occur at roughly -38°C. Looking at the rubbery transition, in sample A, addition of LCP phase shifts the peak to a higher value by 5°C indicating some miscibility between the rubber and LCP. The shift in glass transition temperature depends on weight fraction of miscible components of the blend. EPDM relaxation peak does not exhibit a distinct temperature shift in curve C, due to diluted content of the elastomer in this composition in comparison to curve A. However, intensity of tan δ peak in curve C is lower, indicating better compatibility [6] between LCP and EPDM rubber. As expected, the intensity of tan δ peak for sample B is maximum, indicating least interaction between EPDM and short glass fibers.

Looking at the higher temperature relaxation, the glass transition of toughened nylon 6,6 occurs at around 60°C. The relaxation peak for LCP at 102°C can be seen in Fig. 1 for sample A. For sample C the peaks of nylon 6,6 and LCP are broadened. The extent of compatibilization between nylon 6,6 and LCP appears better in sample C than in sample A.

3.2. Composite morphology

The SEM micrographs of cryo-fractured surface of injection-molded specimens from samples A and C are compared in Fig. 2a and b. In sample A, LCP phase exists as spherical droplets in the core region and some elongated LCP fibrils can be observed towards the skin region where the shear deformation is higher than in the core region. Sample C exhibits a different micromorphology. The LCP phase has extensively elongated into fibrils particularly in the skin region. Good

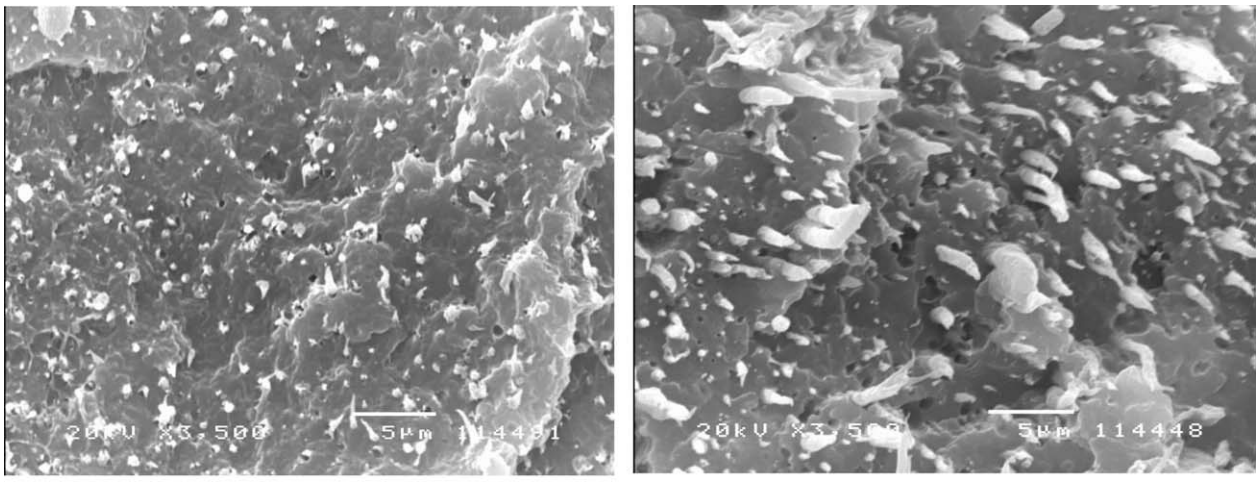

Figure 2 SEM photomicrographs of cryo-fractured specimens of (a) sample A and (b) sample C. LCP fibrillation is evident in sample C.

interfacial adhesion is also evident. Deformation of LCP domains depends on how efficiently shear stress generated from a melt processing operation is transferred onto the LCP phase. Increasing the viscosity of matrix is one route to deliver a higher shear stress for LCP deformation [7]. Addition of glass fibers to toughened matrix increases its melt viscosity during processing. Compatibilization is also a competitive strategy for LCP deformation [8]. We believe higher melt viscosity and improved compatibilization between the LCP and nylon phases, both of which are derived from the hybridization effect [2] in the presence of glass fibers for sample C, contribute to this noteworthy improvement in LCP fibrillation as compared to LCP without glass fibers.

3.3. Characterization of microstructures

Fig. 3 illustrates the microstructures of samples B and C revealed by SEM examination of the polished specimen cross sections. SEM micrographs were taken across the in-plane width (X-Y) perpendicular to the mold filling direction (MFD) of the 6.35 mm-thick Izod specimens. In sample B high concentration of fibers can be observed towards the skin of the specimen. However in sample C, the fiber concentration appears to be sparse towards the side and a distinct middle layer with fibers aligned in the transverse direction to MFD can be seen. Fig. 4 shows the fiber orientation distribution for samples B and C. Sample B exhibits a bimodal distribution with two peaks at 10 degree and 46 degree. Sample C displays a trimodal distribution with peaks at 10, 46 and 78 degrees. Fig. 5 shows the fiber length distributions for samples B and C. From the frequency distribution, number average length (l_n) was calculated using the following equation.

$$\frac{\sum_{i=1}^{n} n_i l_i}{\sum_{i=1}^{n} n_i} \tag{6}$$

where n_i is the number of fibers having a length l_i and $\sum_{i=1}^{n} n_i$ is the total number of fibers measured. For sample B, number average length (l_n) of the fiber was calculated to be 240 μm and for sample C it was 300 μm. Glass fibers retain a higher length in sample C in comparison to sample B.

3.4. Tensile properties

One of the objectives to introduce reinforcements to toughened plastics is to improve the stiffness, which is often reduced by elastomeric inclusions. Fig. 6 shows the representative engineering stress-strain curves for the composites under study. Interestingly, sample A shows considerable elongation after the peak stress. In both samples B and C, the post-yield elongation is significantly reduced. Nevertheless, sample C provides the highest stiffness as indicated in its stress-strain curve. Fig. 7 compares the tensile strength and modulus of the hybrid composites. Tensile strength of sample C is the highest of all compositions. This is consistent with our DMA results, which showed better compatibility between the nylon and LCP phases in comparison to sample A. The good interfacial adhesion between LCP and toughened nylon 6,6 provides better stress transfer from the matrix to reinforcements, which give rise to a higher tensile strength. Weak interfacial adhesion between nylon 6,6 and LCP has resulted in lower tensile strength for sample A. The weakest interfacial adhesion exists in sample B, which shows the lowest tensile strength. The experimental observations in this case are consistent with predictions from composite theory.

Young's modulus increases from 2.9 GPa in sample A to 5.2 GPa in sample C. Sample B exhibits an intermediate value of 3.7 GPa. Stiffness characterizes the initial deformation. In the low strain regime, the interfacial adhesion suffices to transfer the load from the matrix to the discontinuous reinforcements following the Kelly-Tyson's model [9]. Paul and coworkers [10] observed that tensile modulus of glass fiber reinforced composites was relatively independent on the type of silane treatment applied to glass fibers. All the tensile properties reported above (Fig. 7) are higher than the

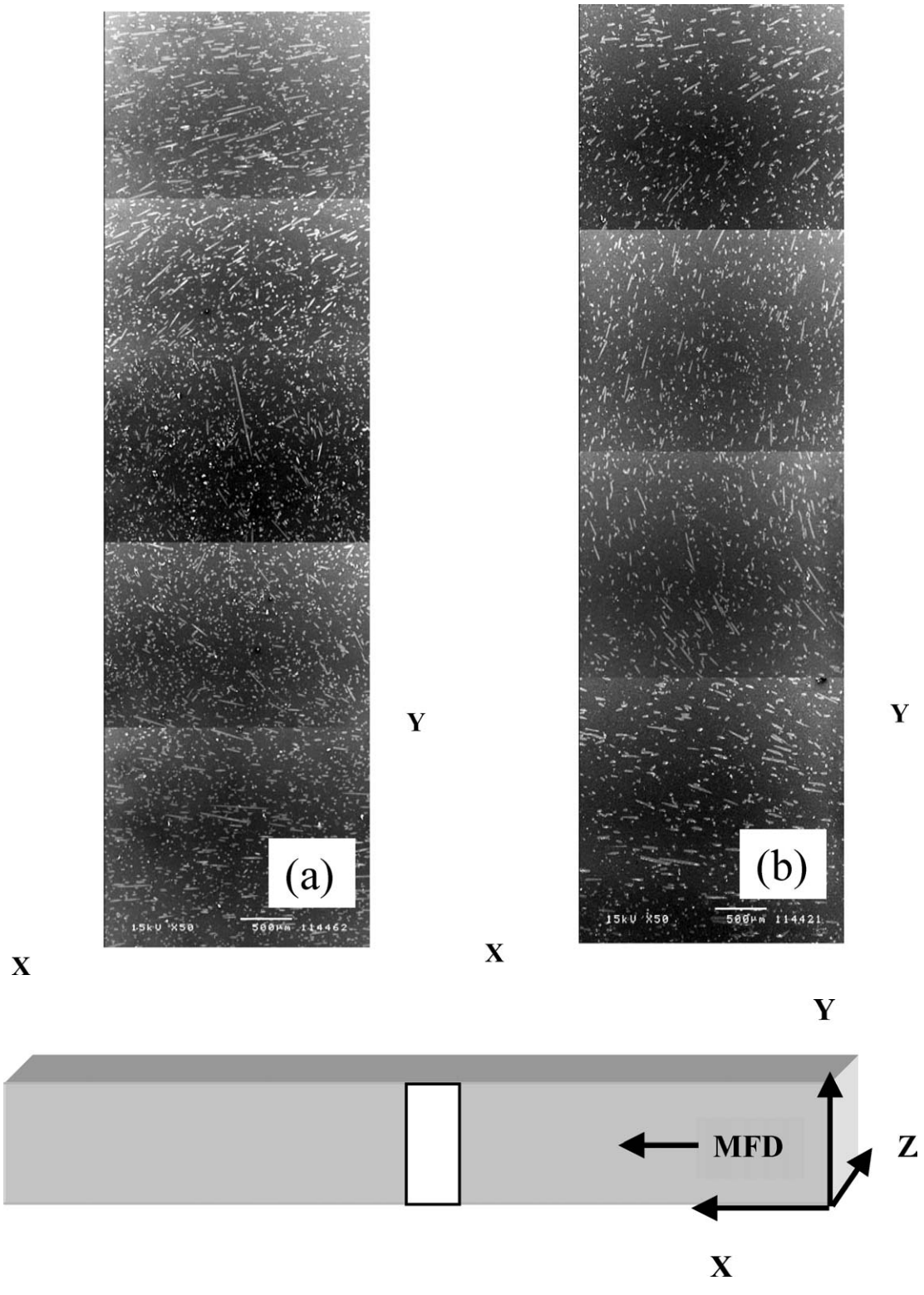

Figure 3 SEM photomicrographs of polished middle section of (a) sample B and (b) sample C. MFD is the mold filling direction.

tensile properties of unreinforced toughened nylon. Our data suggest an engineered combination of mechanical strength, stiffness and toughness is plausible using hybridization method.

3.5. Fracture properties

Typical load-deflection curves for the three samples are shown in Fig. 8. All load-deflection curves indicate some degree of post-yield deformation. The most ductile sample appears to be sample A, which incorporates 20 wt% LCP only in a "supertough" nylon matrix. Upon addition of short glass fibers (sample B), however, the deformation derived from toughened nylon becomes constrained, losing stiffness and flexural strength. The embrittlement effect is understood from Friedrich's microstructural efficiency concept [11], whereby an originally ductile matrix can be embrittled by the presence of glass fibers. Sample C is a hybrid with both fibers and LCP phase. The stiffness has clearly increased but post-yield deformation is more severely constrained. Despite the fruitful information

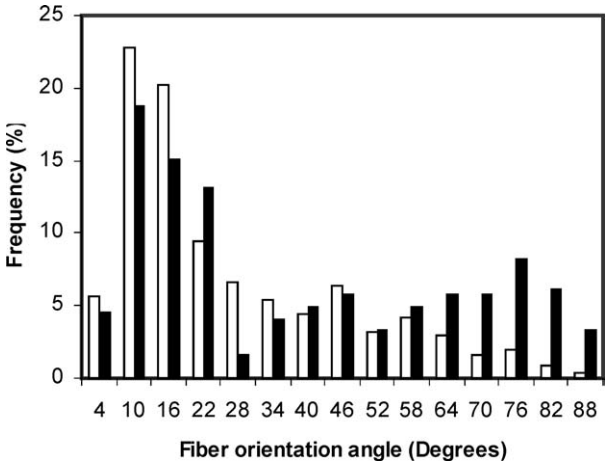

Figure 4 Fiber orientation distribution for sample B (□) and sample C (■).

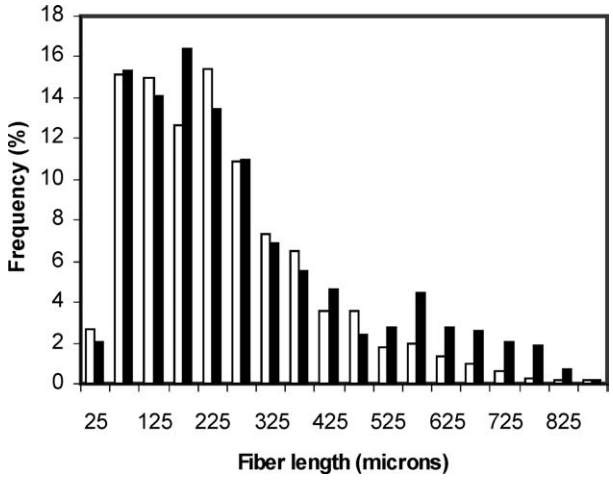

Figure 5 Fiber length distribution for sample B (□) and sample C (■).

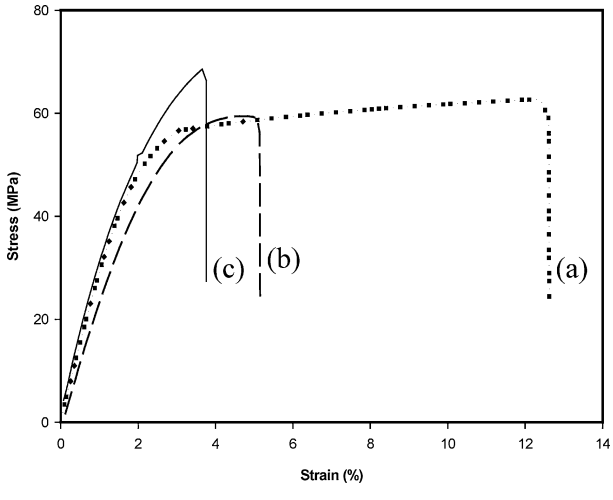

Figure 6 Stress-strain curves of (a) sample A, (b) sample B and (c) sample C.

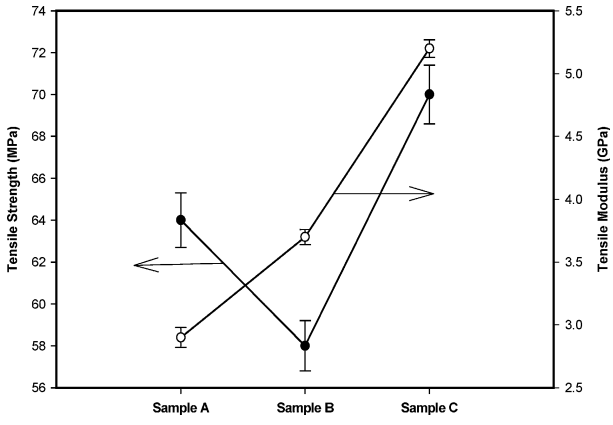

Figure 7 Comparison of tensile strength and modulus for hybrid composites.

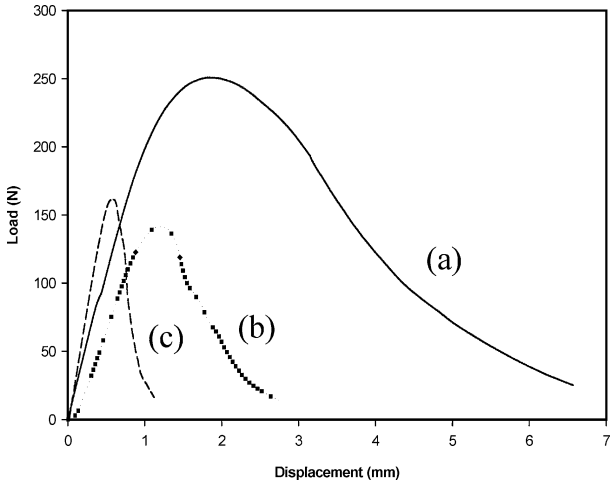

Figure 8 Typical load-displacement curves of (a) sample A, (b) sample B, and (c) sample C.

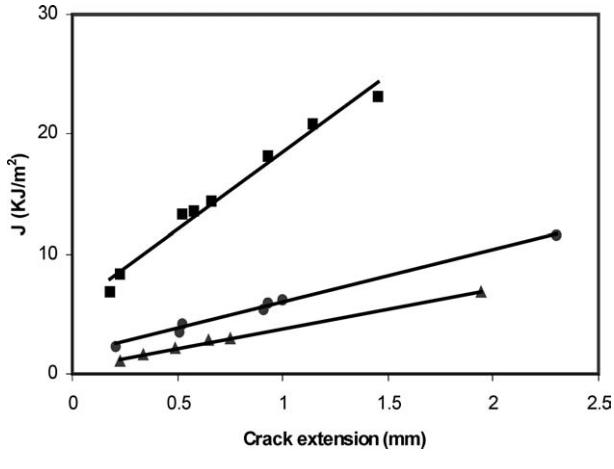

Figure 9 *J-R* curves for hybrid composites: (■) sample A (●) sample B (▲) sample C.

we could obtain from the load-deflection curves for the fracture behavior of the composite samples, we believe a more rigorous fracture mechanics approach to characterize the toughness of the studied materials would be useful.

The crack growth resistance curves for composites are plotted in Fig. 9. Good linearity of J resistance against crack growth is observed for all the compositions with minimal scatter. The crack initiation toughness, J_c, is obtained by extrapolating a linear regression line to zero crack growth [4, 12]. Plane strain conditions can be verified using Equation 2.

Tearing modulus calculated using Equation 3 is indicative of partial propagation component of toughness

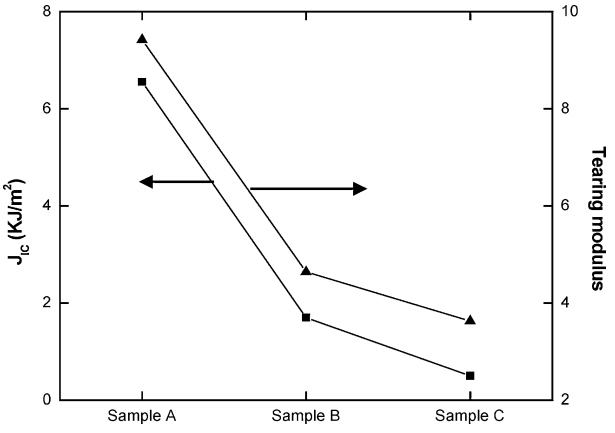

Figure 10 Comparison of J-integral fracture toughness J_{Ic} and tearing modulus T of the hybrid composites.

[13]. Fig. 10 shows the comparisons of J_{Ic} and T for the studied samples. Sample A shows high values in both J_{Ic} and T. The high value (9.42) in T is particularly pronounced. Sample C exhibits the least J_{Ic} and T with intermediate values recorded for sample B. Nevertheless, the value in T is still significant. The R-curve behavior exhibited by the hybrid composite is clearly more desired than neat nylon 6,6, which does not yield any R-curve in crack propagation [13]. The significant crack propagation toughness reinforces the notion that tailored benefits can be obtained with the design for hybrid composites. The measurements of the J_{Ic} and T are consistent with the predictions displayed in the load-deflection curves in Fig. 9.

Fig. 11 shows the w_f versus l plots for the hybrid composites. All the w_f versus l curves show good linearity with some scatter. Note that the EWF technique is uniquely distinct from the multi-specimen J-integral measurements as discussed in Section 2.5 and by the author in ref. [4]. Generally, the w_{Ie} values reported herein are consistent with the measured J_{Ic}. This corroborates our previous findings that w_{Ie} measurements can be used as valid fracture parameters like J_c for composite materials [12].

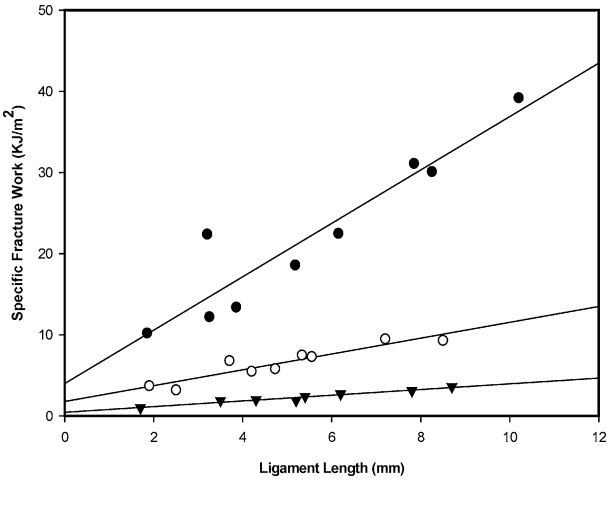

Figure 11 Specific fracture work versus ligament length curves for sample A (●), sample B (○) and sample C (▼).

3.6. Fracture morphology

The SEM micrographs of tested sample A are shown in Fig. 12. The specimen exhibits a stable crack growth region (Fig. 12a). An SEM image of the stable crack growth region at a higher magnification (Fig. 12b) reveals the LCP phase. LCP particles appear to be drawn out of the matrix as fibrils of approximately 2 μm in length, due to interfacial debonding. It appears that, LCP fibrils can bridge the crack faces prior to unstable fracture. The fracture surface also shows interconnected ligaments, which form cavities. It is plausible that the cavities are formed under triaxial tension, which further promote ductile yielding in the ligaments on sample A. The fracture mechanisms as observed under SEM supports the relatively high J_{Ic} and T measured for sample A.

For sample B, the stable crack growth region is diminished in size when compared to sample A (Fig. 13a). This observation is consistent with the stress-shedding mechanisms discussed by Wong and coworkers [14]. The glass fibers take up greater stress in the composite, reducing the matrix stress, which is too small to promote matrix-governed toughening such as rubber cavitation and matrix shear yielding. An enlarged SEM image of the crack growth region (Fig. 13b) shows clean fiber surface, which indicates a weak fiber-matrix interface. According to Friedrich's microstructural efficiency concept [11], such poor interfacial adhesion generally contributes to composite embrittlement. Some plastic deformation can still be observed in the matrix ligaments. Fig. 14a shows the fracture surface for sample C. The stable crack growth region is also small like sample B. In contrast to sample B, however, ductility is further reduced in the ligament region of the matrix. Plastic deformation is severely constrained. In Fig. 14b, spherical droplets of LCP having an average diameter of 3 μm can be seen adhering to matrix. LCP particles appear to be nested in crater-like formation of rubbery phase as if the elastomer has made a coating on LCP. The adhesion between LCP and matrix appears to be stronger. This observation is indicative of a strong interface with good stress transfer from the matrix to the fibers. Under such scenario, toughening can be predicted if the matrix is brittle [11]. However, the matrix investigated is toughened nylon 6,6. It would be anticipated that embrittlement ensues in the studied composite system.

3.7. Overview of hybrid concept

Table II summarizes the hybrid systems investigated in this paper and their potential benefits through hybridization. The primary objective of studying hybrid systems is to investigate if there exists any fundamental benefits in combining materials that serve tailored functions such as better processability, tensile and flexural properties, toughness, electrical and thermal conductivity, and barrier performance in a composite. Ideally, property synergism can be derived from a hybrid system [15]. Synergistic properties are not readily available in combining materials of different functions in one composite. A careful hybrid design and optimization

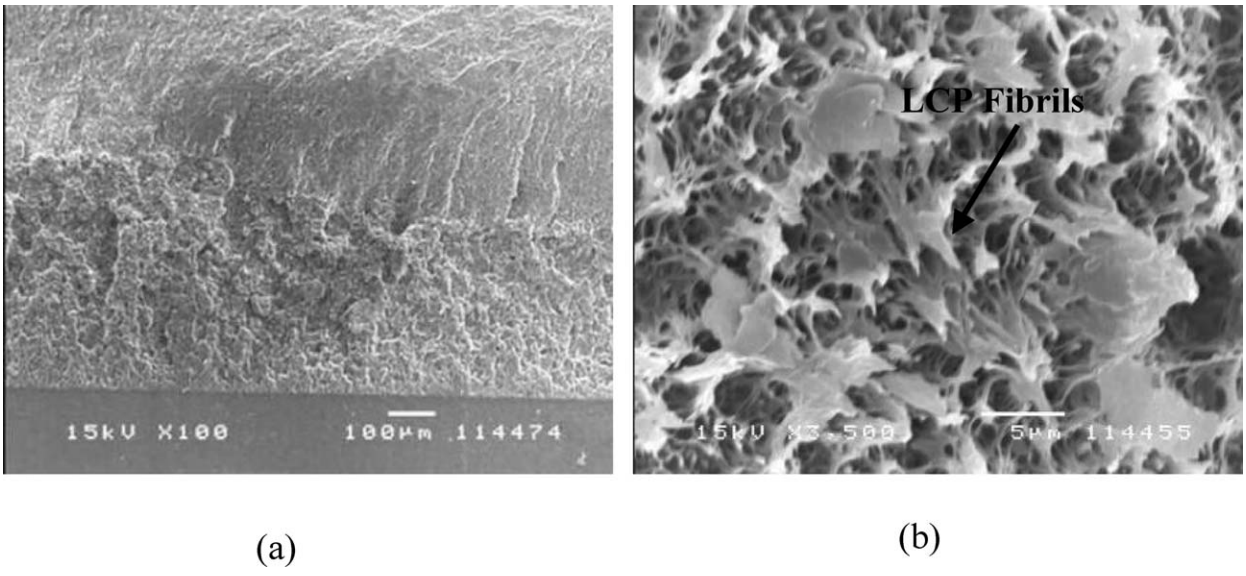

Figure 12 SEM fractographs of sample A: (a) overview of the fracture surface showing the stable crack growth zone; (b) high magnification image taken at the stable crack growth zone. Interfacial debonding of LCP phase is clear.

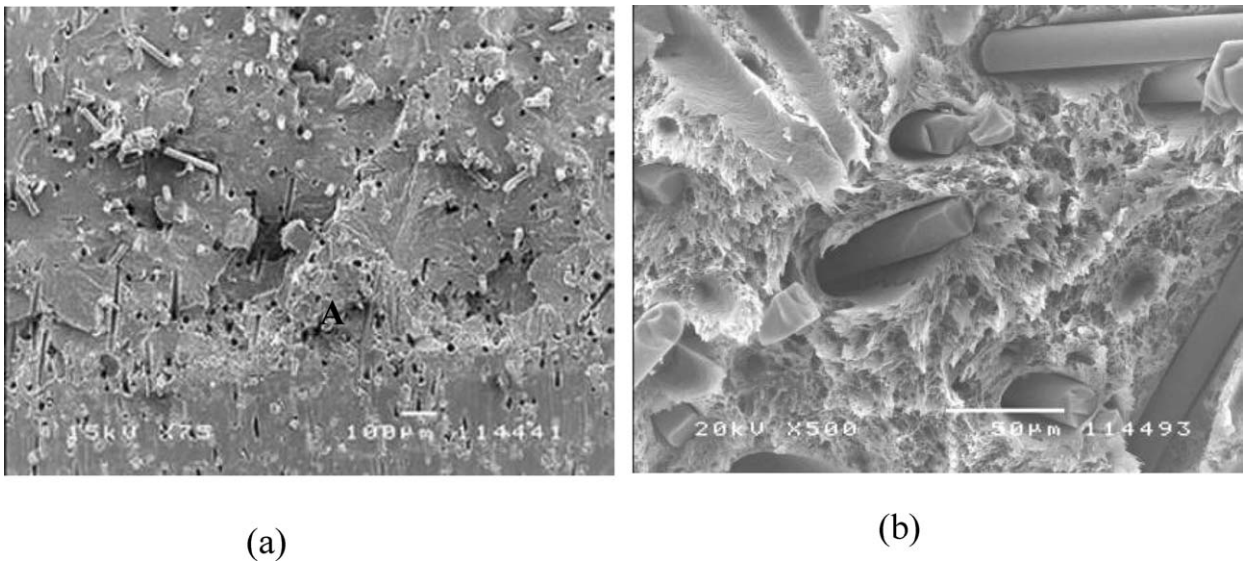

Figure 13 SEM fractographs of sample B: (a) overview of fracture surface; (b) high magnification image taken at the crack growth zone 'A' in (a). Fiber end debonding and consequent localized matrix deformation are shown.

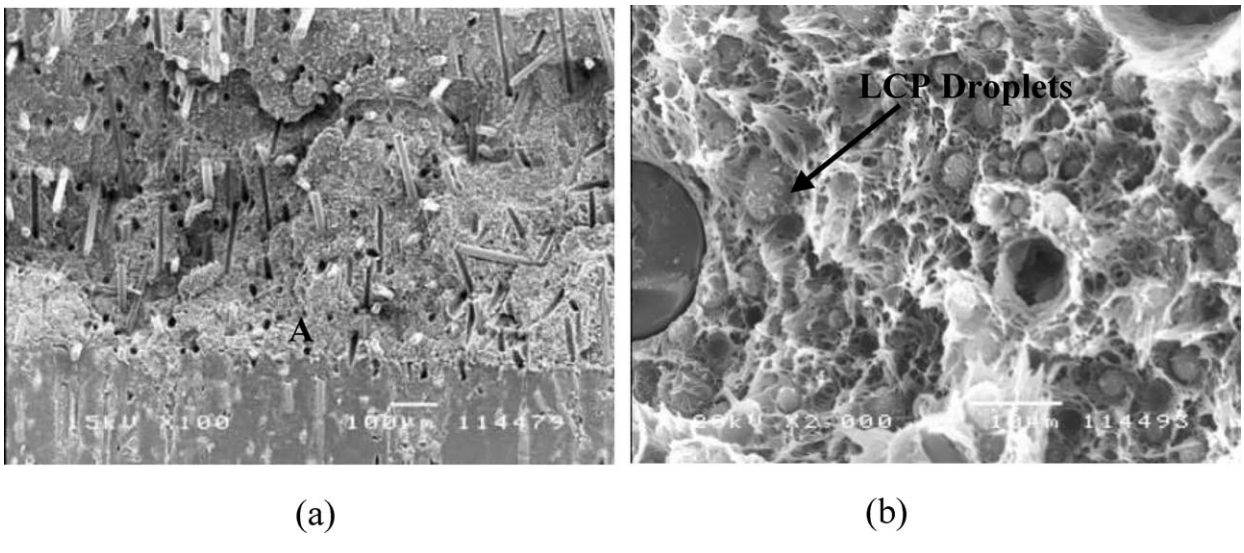

Figure 14 SEM fractographs of sample C: (a) overview of fracture surface and (b) high magnification image taken at the crack growth zone 'A' in (a). Strong interfacial adhesion between nylon 6,6 and LCP is shown.

TABLE II Summary of hybrid effects

Hybrid systems	Microstructural features	Benefits
Sample A	LCP form droplets and sparse fibrils near the skin; extensive matrix deformation	Strength, stiffness from LCP, toughness is sustained by rubber toughening
Sample B	Poor fiber-matrix interface; constrained matrix deformation	Stiffness from glass fiber, Some toughness is sustained by the elastomeric phase.
Sample C	Good fiber-matrix interface; LCP is extensively fibrillated; severely constrained matrix deformation	Processability; thermal stability; good reinforcement effect from glass fibers and LCP fibrils; some propagation component of toughness is maintained.

scheme can often provide tailored benefits in composites development. In this paper, the development of the hybrid composite consisting of LCP and glass fibers in a toughened nylon 6,6 matrix (sample C) can be achieved by adopting two different hybridization routes, namely, (1) combining sample B with LCP and (2) combining sample A with glass fiber. In previous work [1], we observed that addition of LCP to glass fiber reinforced toughened nylon 6,6 (sample B) greatly improved its processability due to the alignment of LCP domains in the direction of flow. We also found that the thermal stability of glass fiber reinforced composites could be considerably enhanced by LCP inclusions. Results in this paper indicated that addition of glass fibers to LCP reinforced toughened nylon 6,6 improved the compatibility between nylon 6,6 and LCP leading to LCP fibrillation. Such fibrillated LCP morphology delivered superior strength and stiffness to sample C, while maintaining some degree of propagation component of toughness. Thus, it is interesting to note that hybridization delivered diverse properties.

4. Conclusions

Three different hybrid composite systems, the compositions of which are given in Table I, were investigated. Based on the presented results, the following conclusions can be drawn:

1. Elastomers compatibilized nylon 6,6 and LCP phase in samples A and C to various degrees. Enhanced compatibilization promoted LCP fibrillation in sample C generating superior tensile strength compared to samples A and B. Sample B exhibited the lowest tensile properties due to poor fiber-matrix adhesion. The results suggested hybridization of toughened nylon 6,6 containing both glass fibers and LCP gave rise to a composite with the highest tensile properties. The property enhancement was attributed to greater compatibility between the LCP and nylon in the presence of maleated elastomer and glass fibers.

2. Two fracture mechanical approaches, J-integral analysis and EWF were employed to assess the fracture behavior of composites. The two techniques gave rather consistent trends and provided a quantitative assessment of the toughness for the studied hybrid composites. Toughness generally decreased as mechanical strength increased for intrinsically ductile polymers. This was understood in light of the Friedrich's microstructural efficiency concept [11] for short fiber reinforced thermoplastics. For a ductile matrix like the "supertough" nylon 6,6, an increase in reinforcement effectiveness reduced the composite toughness. The reduction in toughness could be mechanistically attributed to the stress-shedding mechanism reported earlier [14].

3. Fractographic studies supported the conclusions arising from the measurements in toughness parameters. Ductile stable crack growth was observed in sample A. LCP phase appeared to be drawn out into LCP fibrils due to interfacial debonding. Sample B gave rise to the mechanical strength that was relatively the lowest among the hybrid composites with significant drop in fracture toughness. This suggested glass fiber reinforced toughened nylon did not provide the needed reinforcement as expected but served to reduce the initiation toughness and tearing modulus. Hybridization effect in sample C gave rise to significantly higher tensile properties for toughened matrices. The reduction in fracture toughness was attributed to constrained matrix deformation in the presence of reinforcements as discussed earlier [14].

Acknowledgements

The authors wish to thank Nanyang Technological University (NTU) for funding this work through a graduate research scholarship for one of us (SP). SCW is supported by National Science Foundation SGER Grant # CMS 0335390 administered by the Mechanics and Materials Program and this is greatly appreciated.

References

1. S. PISHARATH and S. C. WONG, *Polym. Comp.* **24** (2003) 109.
2. *Idem.*, *J. Polym. Sci: Polym. Phys.* **41** (2003) 549.
3. D. G. BAIRD, S. S. BAFNA, J. P. DE SOUZA and T. SUN, *Polym. Comp.* **14** (1993) 214.
4. Y. W. MAI, S. C. WONG and X. H. CHEN, in "Polymer Blends Vol. 2: Performance," edited by D. R. Paul and C. B. Bucknall (Wiley-Interscience, New York, 2000) Chap. 20, p. 17.
5. B. MAJUMDAR and D. R. PAUL, in "Polymer Blends Vol. 1: Formulation," edited by D. R. Paul and C. B. Bucknall (Wiley-Interscience, New York, 2000) Chap. 17, p. 539.
6. J. J. SCOBBO, *Polym. Test.* **10** (1991) 279.
7. Y. SEO, *J. Appl. Polym. Sci.* **64** (1997) 359.
8. Y. SEO, S. M. HONG and K. W. KIM, *Macromolecules* **30** (1997) 2978.
9. R. F. GIBSON, "Principles of Composite Material Mechanics" (McGraw-Hill, New York, 1994).
10. D. M. LAURA, H. KESSKKULA, J. W. BARLOW and D. R. PAUL, *Polymer* **43** (2002) 4673.
11. K. FRIEDRICH, *Comp. Sci. Technol.* **22** (1985) 43.

12. S. C. WONG and Y. W. MAI, *Polym. Eng. Sci.* **39** (1999) 356.
13. S. V. NAIR, S. C. WONG and L. A. GOETTLER, *J. Mater. Sci.* **32** (1997) 5335.
14. S. C. WONG, G. X. SUI, C. Y. YUE and Y. W. MAI, *ibid*. **37** (2002) 2659.
15. S. C. WONG and Y. W. MAI, in "Advanced Polymeric Materials," edited by S. G. Advani and G. O. Shonaike (CRC Press, Boca Raton, Florida, 2003) Chap. 12, p. 439.

Received 8 July 2003
and accepted 23 June 2004